NASA/TM—1999-209453

Thermal Barrier Coatings for Advanced Gas Turbine and Diesel Engines

Dongming Zhu
Ohio Aerospace Institute, Cleveland, Ohio

Robert A. Miller
Glenn Research Center, Cleveland, Ohio

National Aeronautics and
Space Administration

Glenn Research Center

October 1999

Available from

NASA Center for Aerospace Information
7121 Standard Drive
Hanover, MD 21076
Price Code: A03

National Technical Information Service
5285 Port Royal Road
Springfield, VA 22100
Price Code: A03

THERMAL BARRIER COATINGS FOR ADVANCED GAS TURBINE AND DIESEL ENGINES

Dongming Zhu
Ohio Aerospace Institute
Cleveland, Ohio 44142
Phone: (216) 433–5422
E-mail: Dongming.Zhu@grc.nasa.gov

Robert A. Miller
Glenn Research Center
Cleveland, Ohio 44135

ABSTRACT

Ceramic thermal barrier coatings (TBCs) have been developed for advanced gas turbine and diesel engine applications to improve engine reliability and fuel efficiency. However, durability issues of these thermal barrier coatings under high temperature cyclic conditions are still of major concern. The coating failure depends not only on the coating, but also on the ceramic sintering/creep and bond coat oxidation under the operating conditions. Novel test approaches have been established to obtain critical thermomechanical and thermophysical properties of the coating systems under near-realistic transient and steady state temperature and stress gradients encountered in advanced engine systems. This paper presents detailed experimental and modeling results describing processes occurring in the ZrO_2-Y_2O_3 thermal barrier coating systems, thus providing a framework for developing strategies to manage ceramic coating architecture, microstructure and properties.

INTRODUCTION

Ceramic thermal barrier coatings (TBCs) have received increasing attention for advanced gas turbine and diesel engine applications. The advantages of using ceramic thermal barrier coatings include increased engine power density, fuel efficiency, and improved engine reliability. As illustrated in Figure 1, because of their low thermal conductivity, thermal barrier coatings can provide better heat insulation for the engine system, thus allowing higher operating temperatures and reduced cooling requirements for future advanced engines. A typical two-layer TBC system consists of a ZrO_2-Y_2O_3 ceramic top coating and an oxidation-resistant metallic bond coat. These thermal barrier coating systems can be applied to the metal substrate either by plasma spray or by electron beam physical-vapor-deposition (EB-PVD) techniques. Figure 2 shows TBC coated engine components-a turbine vane and a diesel engine piston.

Durability issues of these thermal barrier coatings under high temperature cyclic conditions are still of major concern, especially as future engine temperatures increase. The coating delamination failure is closely related to thermal stresses in the coating systems, and oxidation of the bond coat and substrate. Coating shrinkage cracking and ceramic modulus increase resulting from ceramic sintering and creep at high temperatures can further accelerate the coating failure process. In general, the coating failure can occur when the failure driving force is greater than the resistance (Figure 3). Note that in a TBC system, coating delamination driving force increases whereas the resistance decreases with time due to time- and temperature- dependent processes. In order to fully utilize the TBC potential capabilities by taking into account many complex parameters and interactions, advanced coating design tools are of necessity. It is of great importance to establish coating life prediction models and to incorporate the dynamic thermo-mechanical and thermo-physical property information during service, as well as the failure mechanisms under near-realistic transient and steady state temperature and stress gradients encountered in the engine.

The purpose of this paper is to address some of the critical issues such as ceramic sintering and creep, bond coat oxidation, thermal fatigue and their relevance to coating life prediction. Experimental testing techniques have been developed to characterize these thermal barrier coating properties and to investigate the coating failure mechanisms. Emphasis is placed on the dynamic changes of the coating thermal conductivity and elastic modulus, fatigue and creep interactions, and resulting failure mechanisms during the simulated engine tests.

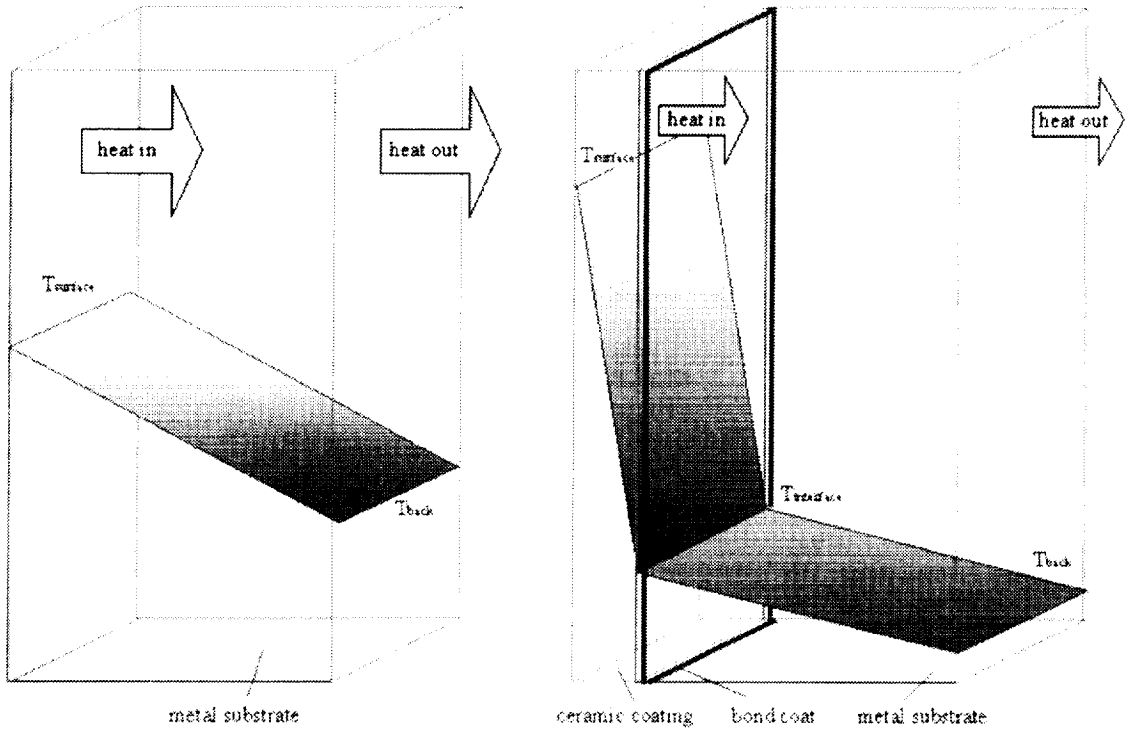

Figure 1 Ceramic thermal barrier coatings provide better heat insulation and protect metal component from oxidation, thus allowing the design of future engines with higher operating temperatures and less cooling requirements.

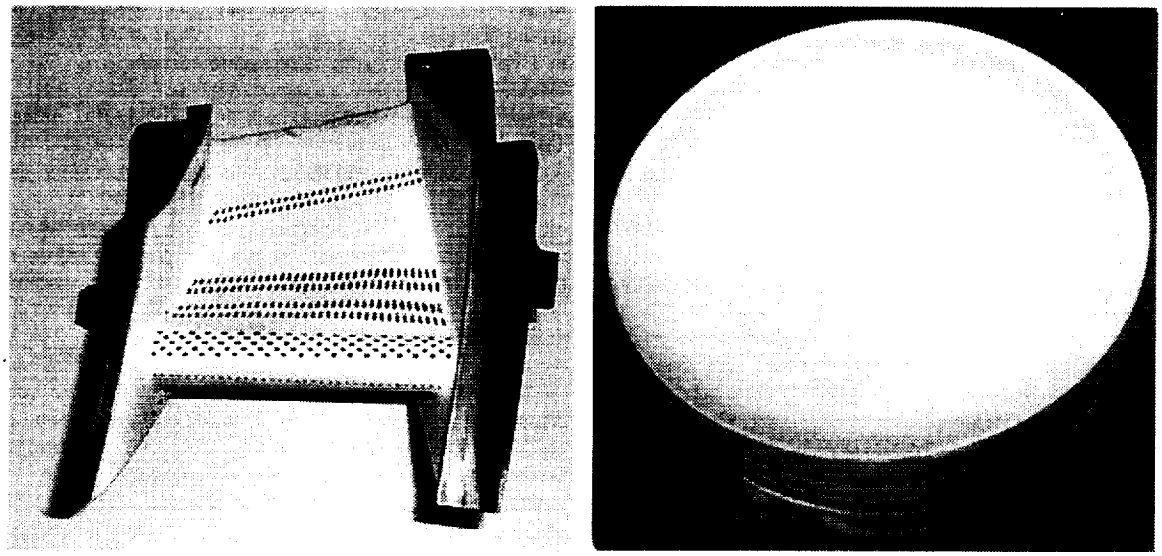

Figure 2 Plasma-sprayed Zirconia-8wt.%Y_2O_3 coatings on engine components of a turbine vane and a diesel engine piston.

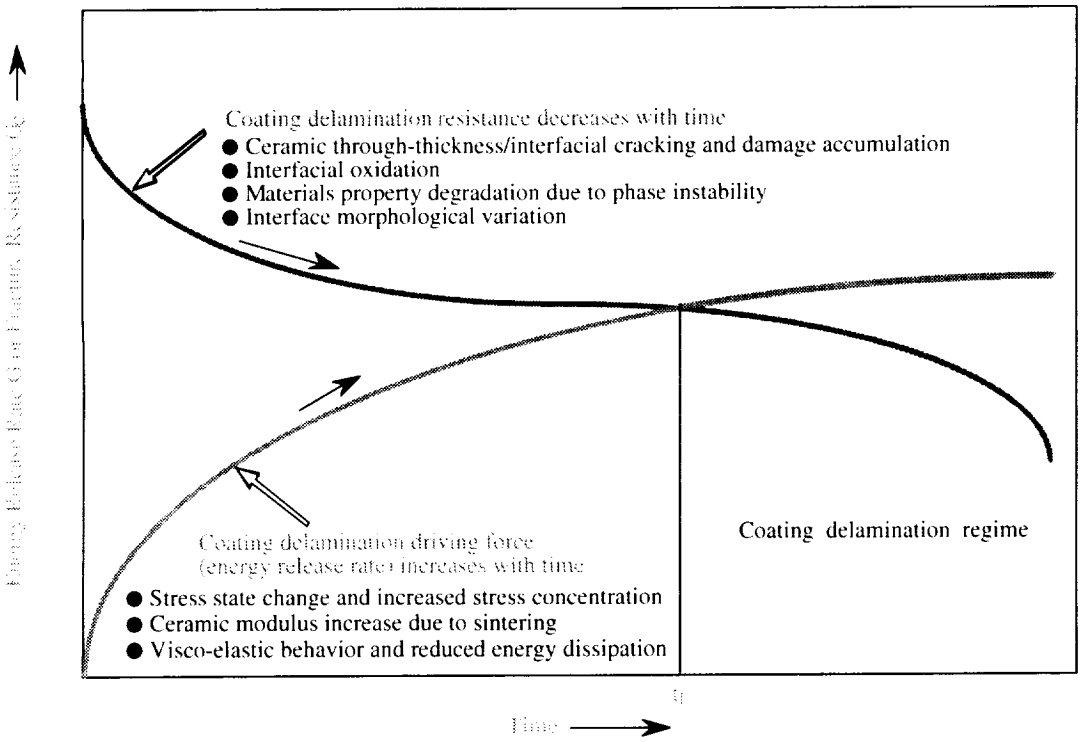

Figure 3 Life prediction of thermal barrier coating systems: a dynamic approach for the dynamic systems. The coating life t_f is determined by coating delamination driving force and resistance.

LIFE PREDICTION ISSUES AND PROPERTY TESTING OF THERMAL BARRIER COATINGS

Sintering and Creep of the Thermal Barrier Coating Systems—Ceramic coating sintering and creep at high temperature are among the most important issues for the development of advanced thermal barrier coatings. It has long been recognized that high temperature coating sintering and creep effects are profound and detrimental to coating performance [1-8]. Not only can sintering and creep result in considerable coating thermal conductivity and elastic modulus increase, but also can cause the coating shrinkage-cracking and eventually the coating spallation.

The sintering and creep mechanisms of the porous, microcracked ceramic thermal barrier coatings are complex. The densification and deformation occurring in thermal barrier coatings at temperature involve the thermally and stress activated diffusion, and the mechanical compacting processes [7, 8]. At a given temperature, the sintering rate of the ceramic coating typically changes with time. Faster shrinkage rates are observed initially, followed by relatively constant and slower rates for longer sintering times. A higher temperature and compressive stress will lead to a higher sintering/creep rate. Figure 4 shows typical sintering and creep characteristics of a plasma-sprayed ZrO_2-8wt% Y_2O_3 coating.

Thermal Conductivity Change Kinetics of Thermal Barrier Coatings—Temperature-dependent change kinetics of the coating thermal conductivity are among the most important parameters required for coating design and life prediction. Increase in thermal conductivity due to ceramic sintering can result in the reduced coating thermal insulation and increased bond coat/substrate oxidation. Therefore, determination of thermal conductivity change kinetics of thermal barrier coatings at high temperature, especially under near-realistic engine temperature and stress gradients, is of great importance.

Figure 5 shows a high power CO_2 laser developed for investigating thermal conductivity change kinetics of the ceramic coating under steady-state heating conditions. This test rig consists of a 3.0 kW CO_2 continuous wave laser (wavelength 10.6 μm), a motor driven rotating test station and temperature measurement instruments such as a thermography system and infrared pyrometers. The laser surface heating and the backside air cooling determine appropriate steady-state temperature gradients across the coating systems. An integrating ZnSe lens combined with the specimen rotation can ensure a uniform laser power distribution for the specimen heating. Overall thermal conductivity changes can thus be continuously monitored in real time by measuring the temperature difference across the ceramic coating.

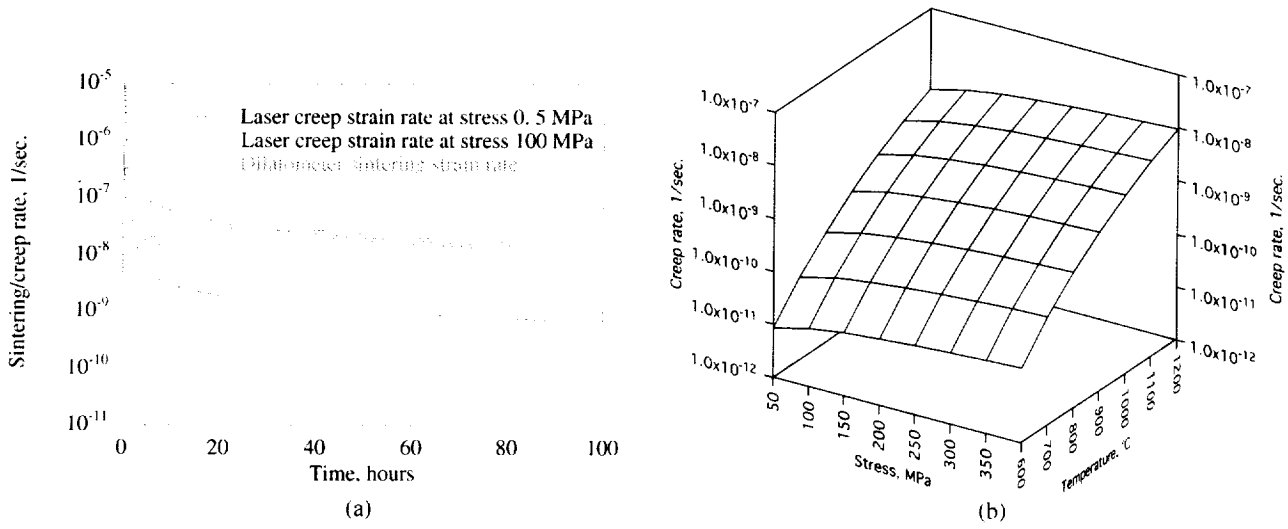

Figure 4 The sintering and creep characteristics of a plasma-sprayed ZrO_2-Y_2O_3 coating material. (a) Sintering and creep rates as a function of time determined by the dilatometer sintering technique and the laser sintering/creep technique. The coating low stress (0.5 MPa) creep rates obtained from the laser creep test are in good agreement with the coating sintering rates obtained from the dilatometer test. (b) Stress- and temperature-dependence of the creep rate for a ZrO_2-8%Y_2O_3 thermal barrier coating (at 500 hours).

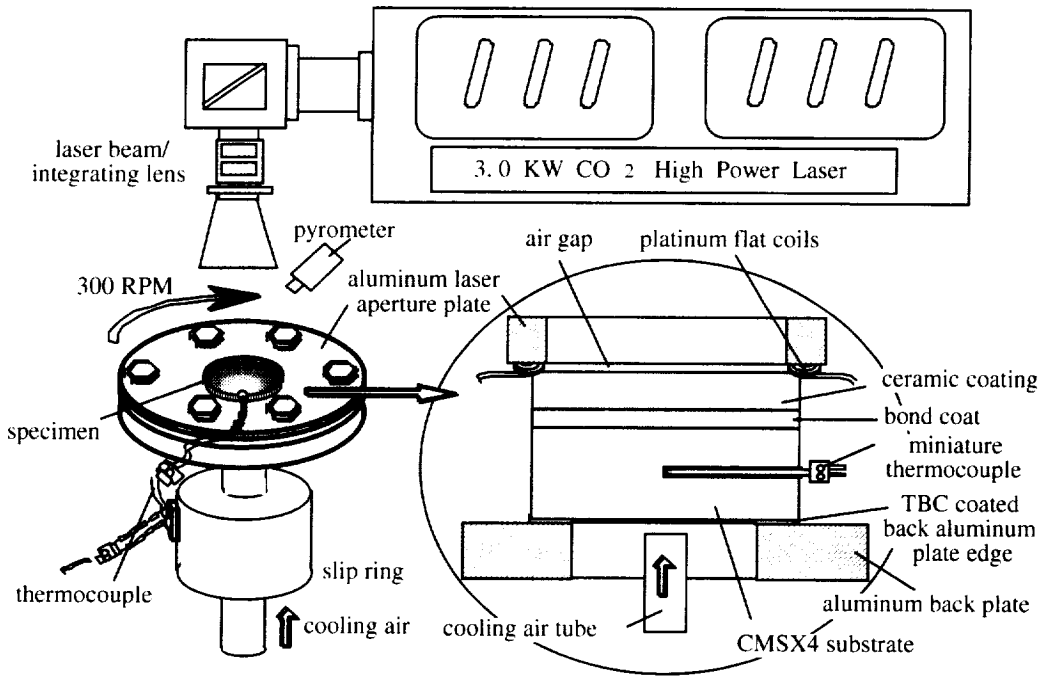

Figure 5 The laser high heat flux rig for determining thermal conductivity change kinetics of thermal barrier coatings. During the test, the ceramic surface and the metal backside temperatures are measured by infrared pyrometers. The metal substrate mid-point temperature can be obtained by an embedded miniature type-K thermocouple. The interfacial temperatures, and the actual heat flux passing through the thermal barrier coating system, are therefore determined under the steady-state laser heating conditions by one-dimensional (one-D) heat transfer models [9].

Figure 6 shows the overall thermal conductivity change kinetics of a 254 μm-thick ZrO_2-Y_2O_3 thermal barrier coating determined by the steady-state laser heat flux testing. Because a thermal conductivity gradient is expected across the ceramic coating under the high thermal gradient conditions (due to the faster thermal conductivity increase near the ceramic surface as compared to near the ceramic/bond coat interface), the observed ceramic thermal conductivity increase reflects an overall effect of the conductivity change in the coating. From the test results shown in Figure 6, the coating thermal conductivity values are increased from the initial value of 1.0 W/m-K to 1.15 W/m-K, 1.19 W/m-K and 1.5 W/m-K after 30 hour testing at the surface temperatures of 990°C, 1100°C, and 1320°C, respectively. The effects of heating time and temperature on the overall ceramic thermal conductivity are approximately described by the ln(k) vs. $L - M$ relationship as shown in Figure 7. The average slope of the Larson-Miller plot for the ZrO_2-Y_2O_3 coating was about 2.93×10^{-5} for the thermal barrier coating system.

Elastic Modulus Evolution under High Heat Flux Conditions—Because of the sintering densification process, the elastic modulus of the porous ceramic coating will increase under the operating conditions [8, 9]. The modulus increase rate will depend upon the actual temperatures and stresses that the coating experiences. Under the high heat flux conditions, however, a significant elastic modulus gradient will be developed and evolve with time. A laser simulated heat flux testing demonstrated that the ceramic coating micro-porosity decreased with increasing laser testing time [8]. The porosity gradients across the coating thickness after laser testing were noticed and correlated to the measured total creep strain gradients. The elastic modulus change kinetics determined by the micro-indentation technique across the coating system are shown in Figure 8. The experimental data can be described by the following relation

$$\frac{E - E_c^{''}}{E_c^{int} - E_c^{''}} = C_t \left\{1 - \exp\left[-\frac{t}{\tau}\right]\right\} \qquad (1)$$

where E is the coating modulus at any given time t, $E_c^{''}$ and E_c^{int} are ceramic coating modulus values at the initial time and at infinitely long time, respectively, τ is relaxation time, C_t is a constant related to temperature and stress in the coating system. It can be seen that a modulus gradient was established in the coating system that evolved with time under the laser imposed temperature and stress gradients. The surface showed very fast modulus increase kinetics. The surface of the ceramic coating reached nearly the assumed final modulus value of 125 GPa in about 20 hours. However, a much longer time is required for the inner layers of the ceramic coating to obtain the final modulus value by laser sintering due to the lower temperatures and stresses under the thermal gradient test conditions.

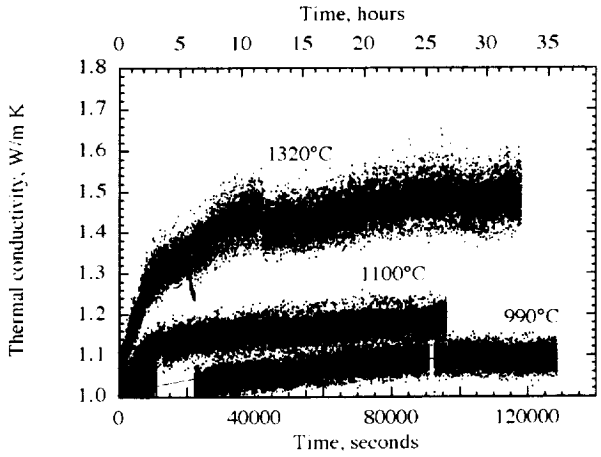

Figure 6 The overall thermal conductivity change kinetics of the ZrO_2-Y_2O_3 thermal barrier coating determined by the real time laser heat flux testing.

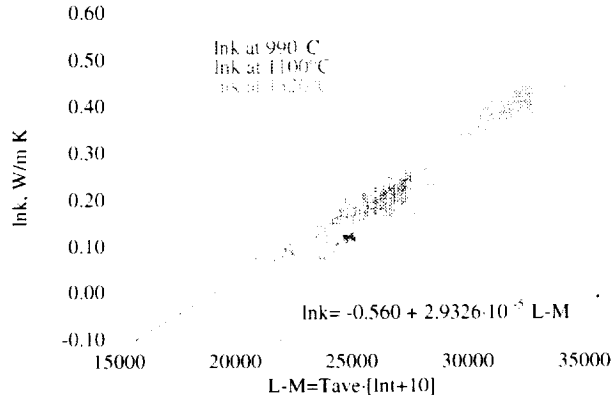

Figure 7 Ceramic thermal conductivity ln(k) as a function of Larson-Miller ($L - M$) parameter ($L - M = T_{ave}[\ln(t)+C]$, where t is the heating time in seconds and T_{ave} is the average temperature in Kelvin in the ceramic coating, C is a fitting constant, and C=10 in this study). The effects of heating time and temperature on the overall ceramic thermal conductivity are approximately described by the conductivity - Larson-Miller relationship.

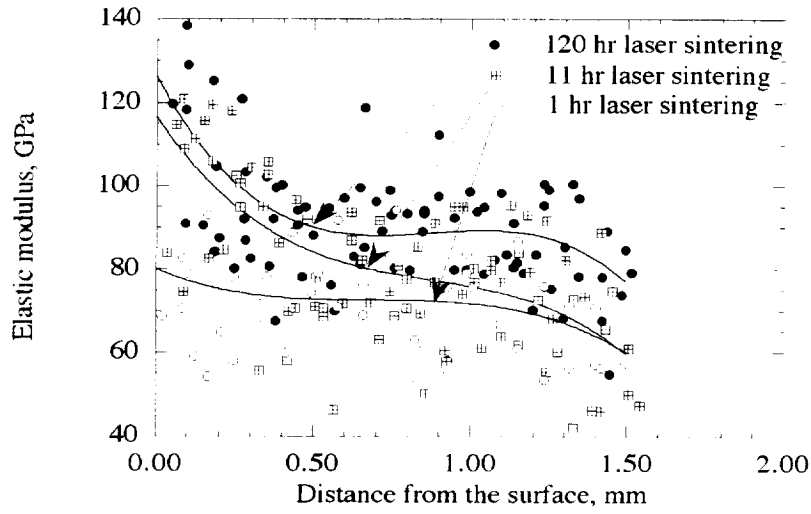

(a)

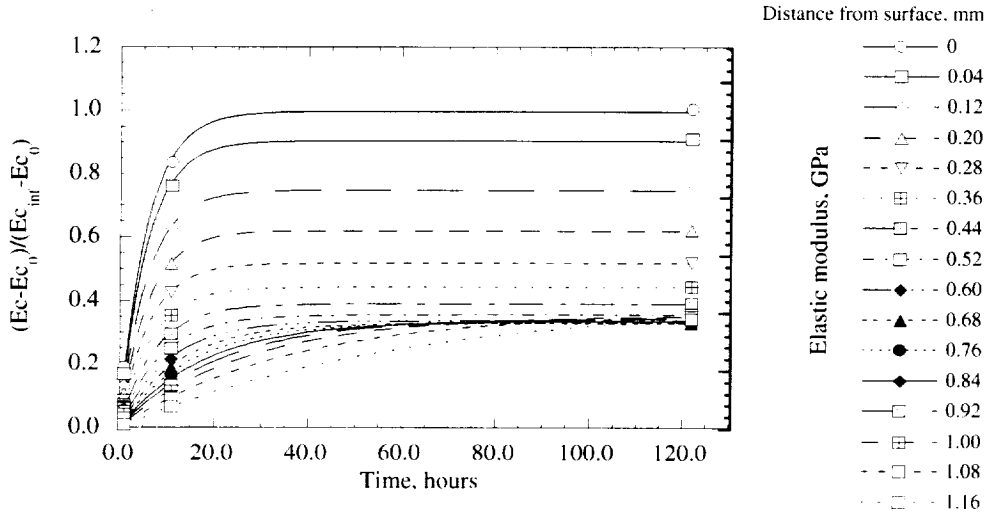

(b)

Figure 8 Elastic modulus evolution in a ZrO_2-Y_2O_3 thermal barrier coating under laser heat flux sintering and creep conditions. (a) The elastic modulus distributions in the ZrO_2-Y_2O_3 thermal barrier coating as a function of laser sintering time. (b) The experimentally determined modulus change kinetics across the coating system.

Oxidation of Bond Coats and Ceramic/Bond Coat Adhesion—The plasma-sprayed bond coats, especially the air plasma-sprayed bond coats, can exhibit a complicated transient oxidation behavior during the early stage of oxidation due to its relatively high porosity. However, the oxidation of these bond coats will follow approximately a parabolic rate law after this transient stage. Therefore, the Al_2O_3 scale growth kinetics of the NiCrAlY and FeCrAlY type bond coats can be described by the apparent parabolic rate constant k_p using the following relationship

$$(\Delta w)^2 = w_0^2 + k_p t \qquad (2)$$

where Δw is the specific weight gain in mg/cm^2, and w_0 is a constant (in mg/cm^2) to account for the fact that the parabolic behavior only occurs after the initial transient period. The oxidation kinetics and Arrhenius plot of the parabolic rate constants for an air plasma-sprayed Ni-36Cr-5Al-Y bond coat are illustrated in Figure 9. The oxidation of bond coats can cause the interfacial damage. As shown in Figure 10, the oxide scale growth at the ceramic/bond coat interface initiated the cracking and separation at the ceramic/bond coat interface. The interfacial adhesion can be significantly reduced due to the severe bond oxidation [10].

In order to quantify the ceramic/bond coat adhesion after oxidation, coating pull-adhesion experiments have been carried out. Figure 11 shows a schematic diagram of the adhesion tester and the specimen configuration. In the test, a 25.4 mm diameter specimen with an interfacial center penny-shaped flaw (flaw diameter $2a$ = 4.366mm) is pre-oxidized and then tested in the adhesion tester. The load is gradually increased and the critical load for coating de-bonding is recorded. The energy release rate for this specimen configuration can be expressed by

$$G = 2\pi\varepsilon(1+\varepsilon^2)\left(\frac{b^2-d^2}{d}\right)a\sigma \qquad (3)$$

where

$$\varepsilon = \frac{1}{2\pi}\ln\left(\frac{(3-4\upsilon_m)E_c + E_m}{E_c + (3-4\upsilon_c)E_m}\right) = \frac{1}{2\pi}\ln\left(\frac{b+d}{b-d}\right) \qquad (3a)$$

$$b = \frac{1}{2\pi}\left(\frac{1-\upsilon_c}{E_c} + \frac{1-\upsilon_m}{E_m}\right) \qquad (3b)$$

$$b = \frac{1}{4\pi}\left(\frac{1-2\upsilon_c}{E_c} - \frac{1-2\upsilon_m}{E_m}\right) \qquad (3c)$$

and E_c, υ_c, E_m, υ_m are the Young's moduli and Poisson's ratios for the ceramic coating and metal substrate, respectively. The test results for a ZrO_2-8%Y_2O_3/Ni-36Cr-5Al-Y bond coat system oxidized at 1100°C are shown in Figure 12.

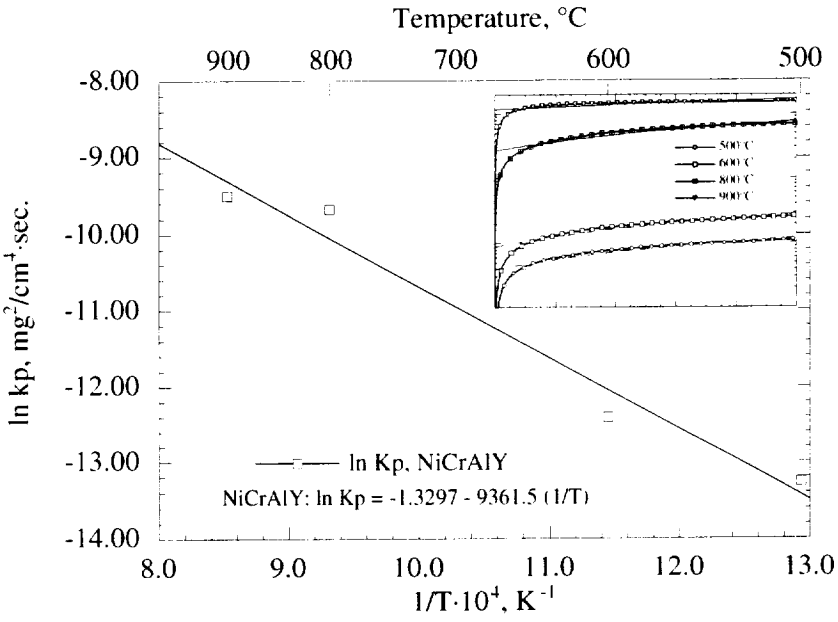

Figure 9 The oxidation kinetics of an air plasma-sprayed Ni-36Cr-5Al-Y bond coat determined by thermogravimetric analysis (TGA).

(a)

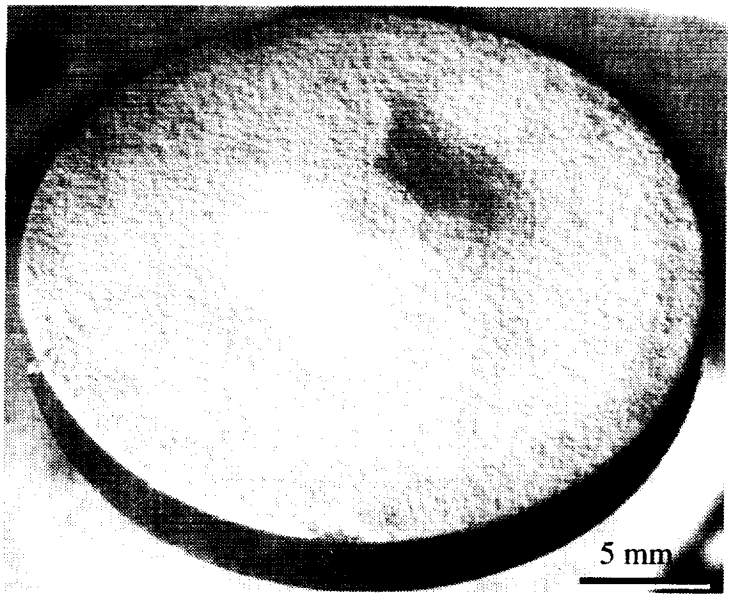

(b)

Figure 10 Bond coat oxidation induced coating delamination and spallation. (a) The coating cracking and separation at the ceramic/bond coat interface in a ZrO_2-8wt%Y_2O_3/NiCrAlY bond coat/IN792 substrate system, after 50 hour furnace oxidation at 1100°C in air. (b) The ceramic coating delamination and buckling in a ZrO_2-8wt%Y_2O_3/NiCrAlY bond coat/CMSX-4 substrate system due to the reduced interfacial adhesion, after 35 hour laser high heat flux testing (interface temperature approximately 1100°C).

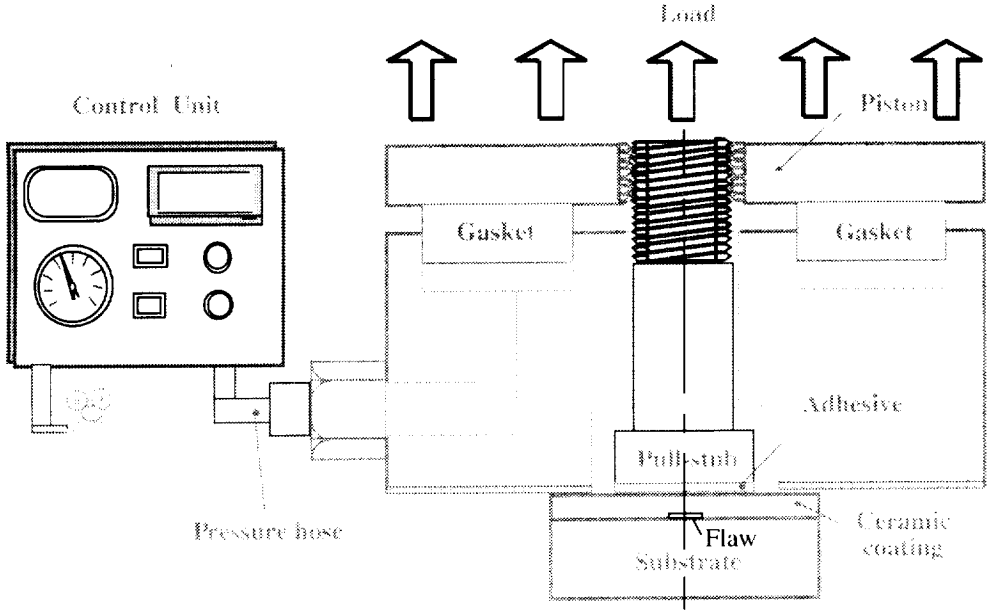

Figure 11 Schematic diagram showing the adhesion tester and specimen configurations.

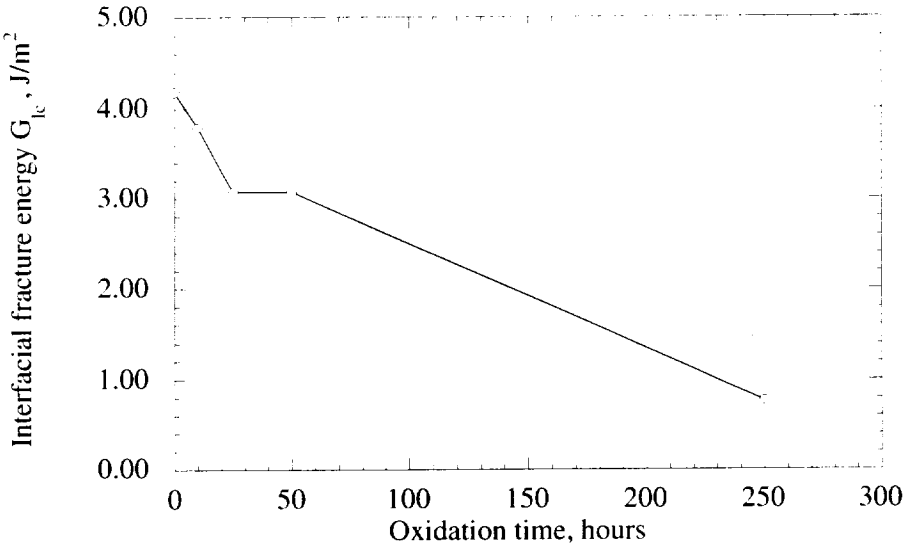

Figure 12 Ceramic/bond coat interfacial fracture energy as a function of oxidation time for a ZrO_2-8%Y_2O_3/Ni-36Cr-5Al-Y bond coat/CMSX-4 substrate system oxidized at 1100°C. (Mechanical properties used for the critical energy release rate calculation: $E_c = 30GPa$, $E_m = 190GPa$, $\upsilon_c = 0.25$, $\upsilon_m = 0.27$).

Thermal Fatigue Behavior of Thermal Barrier Coatings—Thermal barrier coating systems experience severe thermal fatigue during engine operation. The thermal fatigue results from the thermal stresses from thermal cycling and/or thermal transients encountered in an engine. The coating thermal fatigue failure is related not only to coating thermal expansion mismatch, and oxidation of the bond coats and substrates, but also to the steep thermal stress gradients induced in the coating systems.

Thermal fatigue behavior of thermal barrier coatings has been thoroughly investigated under simulated diesel engine thermal transients [11, 12]. In a diesel engine, typically two types of thermal fatigue transients exist. The first type of transient, which is associated with the start/stop and no-load/full-load engine cycle, generates thermal low cycle fatigue (LCF) in the coating system. The second transient type, which is associated with the in-cylinder combustion process, generates a thermal high cycle fatigue (HCF) with typical frequency on the order of 10 Hz (i.e., 1000-2600 RPM). The HCF transient can induce a temperature fluctuation of more than 200°C that will be superimposed onto the steady-state engine temperature at the coating surface. Under the complex thermal LCF and HCF conditions, the LCF mechanism in the thermal barrier coatings is primarily associated with the coating sintering and creep at high temperature, whereas the HCF mechanism is closely associated with the cyclic stresses originating from the high frequency temperature fluctuation at the ceramic coating surface. The sintering and creep strains in the ceramic coating under high temperature thermal gradient conditions will lead to a tensile stress state during cooling, thus providing the major driving force for the vertical crack growth under LCF conditions. The HCF thermal loads act on the crack by a wedging mechanism, resulting in the accelerated crack growth and coating delaminations [12]. Figure 13 shows a typical surface vertical crack propagation near the ceramic/bond coat interface, and initiating the coating delamination.

The crack growth behavior of the ceramic coatings has been determined under laser simulated LCF and HCF conditions [6, 12]. During a superimposed thermal LCF-HCF testing, the surface vertical crack in the thick thermal barrier coating can propagate under both LCF and HCF loads according to [12]

$$\left(\frac{da}{dN}\right)_{LCF} = C_1 \left(\Delta K_{ILCF}\right)^m + \int_0^{N^*_{HCF}} C_2 \left(\Delta K_{IHCF}\right)^m dN_{HCF} \qquad (4)$$

where a is the crack length, m, C_1 and C_2 are constants, N^*_{HCF} is the characteristic HCF number, ΔK_{ILCF} and ΔK_{IHCF} are stress intensity factor amplitudes of the crack under LCF and HCF loads, respectively. The stress intensity factor amplitudes are functions of crack geometry, crack length, stress magnitudes and distributions, thus being closely associated with the coating sintering, creep, oxidation and related material property changes.

As shown in Figure 14, the measured crack length in the ceramic coating system increases with the LCF cycle number and surface temperature. The HCF component further increases the overall coating crack length. The fatigue crack growth rate in the ceramic coating strongly depends on the characteristic HCF cycle number, N^*_{HCF}, which is defined as HCF cycle numbers per LCF cycle. As illustrated in Figure 15, the average fatigue crack growth rate increases with the characteristic HCF cycle number. The increased crack growth rate in the ceramic coating with characteristic cycle number is attributed to the HCF interaction effect and increased sintering effect due to longer heating cycle or higher temperature. The experiments demonstrate the strong interactions between LCF, HCF, ceramic coating sintering and creep.

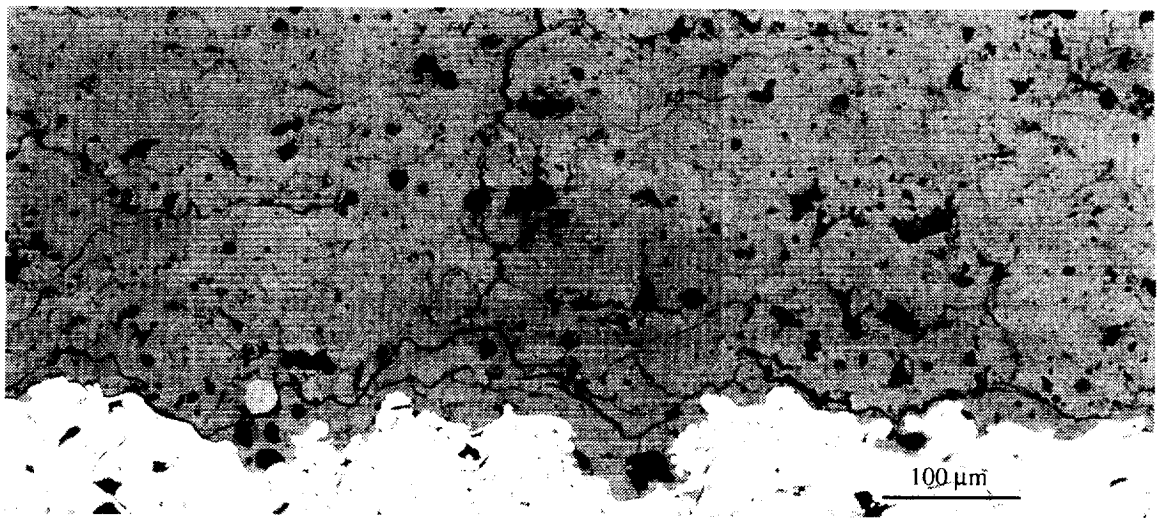

Figure 13 A surface vertical crack propagation and coating delamination under the laser heat flux induced thermal fatigure loads.

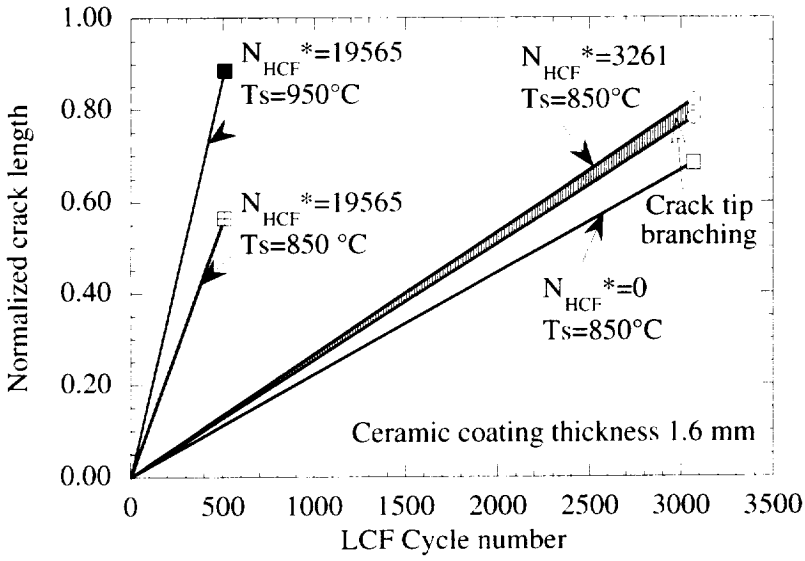

Figure 14 The crack length (normalized to the coating thickness) as functions of LCF and characteristic HCF numbers. For given LCF and HCF cycle numbers, longer crack length was obtained at surface temperature 950°C as compared at 850°C. The crack growth rates with respect to LCF cycle are assumed to be linear under various LCF and HCF test conditions, and therefore is represented by the slopes of these straight lines.

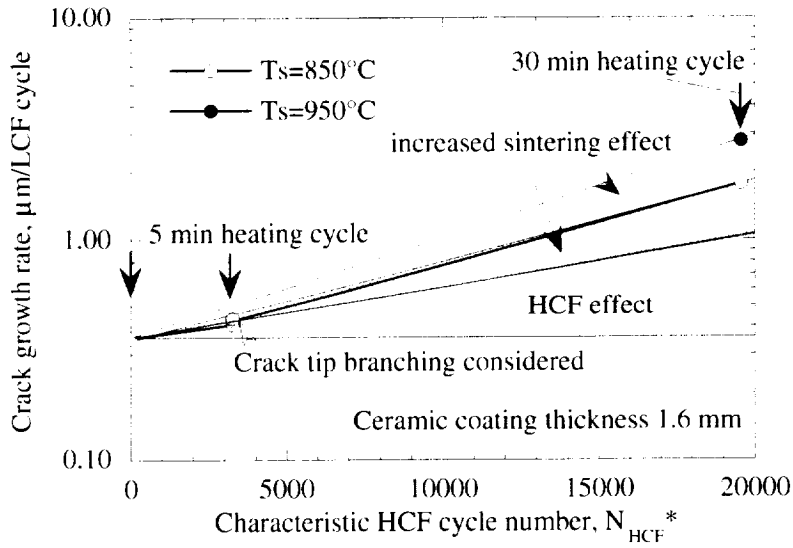

Figure 15 Crack growth rate as a function of characteristic HCF cycle number (HCF numbers per LCF cycle), N^{*}_{HCF}. With the fixed HCF frequency, the increased crack growth rate in the ceramic coating with characteristic cycle number is attributed to the pure HCF interaction effect and increased sintering effect due to longer heating cycle or higher temperature.

CONCLUDING REMARKS

This paper presents important thermal barrier coating design and life prediction issues such as ceramic sintering and creep, thermal conductivity and elastic modulus change kinetics, bond coat oxidation and the ceramic coating thermal fatigue. Experimental techniques have been developed to characterize important thermo-physical and thermo-mechanical properties of thermal barrier coating systems, and to investigate the failure mechanisms under near-realistic engine conditions. The test results will help to better understand the coating failure processes and establish mechanism- and thermal fatigue-based coating life prediction models.

REFERENCES

[1] R. F. Firestone, W. R. Logan, and J. W. Adams, "Creep of Plasma Sprayed Zirconia," NASA Lewis Research Center,, Cleveland, Ohio NASA CR-167868, 1982.

[2] H. E. Eaton and R. C. Novak, "Sintering Studies of Plasma-Sprayed Zirconia," *Surface and Coatings Technology*, vol. 32, pp. 227-236, 1987.

[3] S. M. Meier, D. M. Nissely, and K. D. Sheffler, "Thermal Barrier Coating Life Prediction Model Development: Phase II-Final Report," NASA Lewis Research Center, Cleveland, OH NASA-CR 182230, 1991.

[4] H. E. Eaton, J. R. Linsey, and R. B. Dinwiddie, "The Effect of Thermal Aging on the Thermal Conductivity of Plasma Sprayed Fully Stabilized Zirconia," presented at Thermal Conductivity, 1994.

[5] J. G. Goedjen, W. J. Brindley, and R. A. Miller, "Sintering of Plasma-Sprayed Sol gel Zirconia-Yttria as a Function of Silica Content," presented at Advances in Thermal Spray Science and Technology, Houston, Texas, 1995.

[6] D. Zhu and R. A. Miller, "Investigation of Thermal Fatigue Behavior of Thermal Barrier Coating Systems," *Surface and Coatings Technology*, vol. 94-95, pp. 94-101, 1997.

[7] D. Zhu and R. A. Miller, "Sintering and Creep Behavior of Plasma-Sprayed Zirconia and Hafnia-Based Thermal Barrier Coatings," *Surface and Coatings Technology*, vol. 108-109, pp. 114-120, 1998.

[8] D. Zhu and R. A. Miller, "Determination of Creep Behavior of Thermal Barrier Coatings under Laser Imposed High Thermal and Stress Gradient Conditions," *Journal of Materials Research*, vol. 14, pp. 146-161, 1999.

[9] D. Zhu and R. A. Miller, "Thermal Conductivity and Elastic Modulus Evolution of Thermal Barrier Coatings Under High Heat Flux Conditions," NASA Glenn Research Center, Cleveland, Ohio NASA TM-209069, April 1999.

[10] D. Zhu and R. A. Miller, "Evaluation of Oxidation Damage in thermal Barrier Coatings," NASA Lewis Research Center, Cleveland, Ohio NASA TM-107360, 1996.

[11] D. Zhu and R. A. Miller, "Influence of High Cycle Thermal Loads on Thermal Fatigue Behavior of Thick Thermal Barrier Coatings," NASA Lewis Research Center, Cleveland, Ohio NASA TP-3676, May 1997.

[12] D. Zhu and R. A. Miller, "Investigation of Thermal High Cycle and Low Cycle Fatigue Mechanisms of Thick Thermal Barrier Coatings," *Materials Science and Engineering*, vol. A245, pp. 212-223, 1998.

REPORT DOCUMENTATION PAGE

Form Approved
OMB No. 0704-0188

1. AGENCY USE ONLY (*Leave blank*)	2. REPORT DATE	3. REPORT TYPE AND DATES COVERED
	October 1999	Technical Memorandum

4. TITLE AND SUBTITLE

Thermal Barrier Coatings for Advanced Gas Turbine and Diesel Engines

5. FUNDING NUMBERS

WU-523-21-13-00

6. AUTHOR(S)

Dongming Zhu and Robert A. Miller

7. PERFORMING ORGANIZATION NAME(S) AND ADDRESS(ES)

National Aeronautics and Space Administration
John H. Glenn Research Center at Lewis Field
Cleveland, Ohio 44135-3191

8. PERFORMING ORGANIZATION REPORT NUMBER

E-11948

9. SPONSORING/MONITORING AGENCY NAME(S) AND ADDRESS(ES)

National Aeronautics and Space Administration
Washington, DC 20546-0001

10. SPONSORING/MONITORING AGENCY REPORT NUMBER

NASA TM—1999-209453

11. SUPPLEMENTARY NOTES

Prepared for the NATO Fall 1999 Meeting, Applied Vehicle Technology Panel, sponsored by the NATO Research and Technology Agency, Ottawa, Canada, October 18–21, 1999. Dongming Zhu, Ohio Aerospace Institute, 22800 Cedar Point Road, Cleveland, Ohio 44142; and Robert A. Miller, NASA Glenn Research Center, Cleveland, Ohio. Responsible person, Dongming Zhu, organization code 5160, (216) 433–5422.

12a. DISTRIBUTION/AVAILABILITY STATEMENT

Unclassified - Unlimited
Subject Categories: 24 and 25 Distribution: Nonstandard

This publication is available from the NASA Center for AeroSpace Information, (301) 621-0390.

12b. DISTRIBUTION CODE

13. ABSTRACT ***(Maximum 200 words)***

Ceramic thermal barrier coatings (TBCs) have been developed for advanced gas turbine and diesel engine applications to improve engine reliability and fuel efficiency. However, durability issues of these thermal barrier coatings under high temperature cyclic conditions are still of major concern. The coating failure depends not only on the coating, but also on the ceramic sintering/creep and bond coat oxidation under the operating conditions. Novel test approaches have been established to obtain critical thermomechanical and thermophysical properties of the coating systems under near-realistic transient and steady state temperature and stress gradients encountered in advanced engine systems. This paper presents detailed experimental and modeling results describing processes occurring in the ZrO_2-Y_2O_3 thermal barrier coating systems, thus providing a framework for developing strategies to manage ceramic coating architecture, microstructure and properties.

14. SUBJECT TERMS

Thermal barrier coatings; Life prediction; Thermal conductivity; Interfacial adhesion

15. NUMBER OF PAGES

18

16. PRICE CODE

A03

17. SECURITY CLASSIFICATION OF REPORT	18. SECURITY CLASSIFICATION OF THIS PAGE	19. SECURITY CLASSIFICATION OF ABSTRACT	20. LIMITATION OF ABSTRACT
Unclassified	Unclassified	Unclassified	